Supporting information

Durable, Rate Capable and High Energy Hybrid Supercapacitor From PANI/ZnO/SnO2 Nanocomposite with Zero-Waste Electrolyte Approach

Aranganathan Viswanathan* and Vanchiappan Aravindan*

Department of Chemistry, Indian Institute of Science Education and Research (IISER), Tirupati-517619, Andhra Pradesh, India.

Corresponding authors: ranguchemist@gmail.com and aravind.van@gmail.com

S1. Synthesis of PANI and its by-product

The synthesis of PANI is the well-known method of oxidative polymerization. In the typical synthesis, 1 mL of aniline was dispersed in 200 mL of distilled water, followed by the addition of 3.1 g of ammonium persulphate and the reaction mixture was stirred at room temperature for 5 hrs. Then, the green PANI and its liquid by-products were separated by centrifugation. This liquid by-product of PANI was used as an electrolyte for the PZnSn, which is abbreviated as SLP in the manuscript.

S2. Characterization details

The IR spectra of PZnSn were recorded using the ATR setup of FT-IR Perkin Elmer spectrophotometer (brand- L1600300 Spectrum TWO LiTa(serial No.- 117460)). The powder–XRD spectra (Rigaku D/teX Ultra 250 diffractometer) using Cu Kα (λ=1.54 Å) at 40 kV and 200 mA, FE-SEM images and EDS spectra were recorded using a field emission microscope (Carl Zeiss Strasse 22) and EDAX (model – ELECT PLUS (serial No.:31261), respectively. X-ray Photoelectron Spectroscopy (XPS) measurements were carried out using the theta probe AR-XPS

system, Thermo Fisher Scientific, UK after the internal standard C1s peak was corrected as 284.6 eV. The survey spectrum was recorded at the pass energy of 70 eV and individual core spectra were recorded at the pass energy of 40 eV. Raman spectra were recorded (400–4000 cm^{-1}) using Horiba Yvon Jobin microscope (Labram hr800, wavelength of laser-532 nm). Electrochemical characterizations of electrode material were carried out at a potential range of 0-1.2 V by cyclic voltammetry (CV), galvanostatic charge/discharge (GCD) and electrochemical impedance spectroscopy (EIS) (frequency range of 100 k Hz - 0.01 Hz at open circuit potential with an AC perturbation amplitude of 10 mV) using two electrode systems with 1 M H_2SO_4 and SLP as the electrolytes (Ametek-VersaSTAT3 (Princeton Applied Research)).

S3. Fabrication details

The as-synthesized PZnSn were fabricated as symmetric supercapacitor devices following the method reported in [4,5]. In this procedure, a pair of carbon fabric of dimensions 2 cm × 2 cm was coated with electrode material by drop casting, a Whatman filter paper (Cat. No.-1001 125) (2 cm × 2 cm) was used as a dielectric material, and a pair of stainless-steel plates nearly of same dimensions of carbon fabric are used as current collectors.

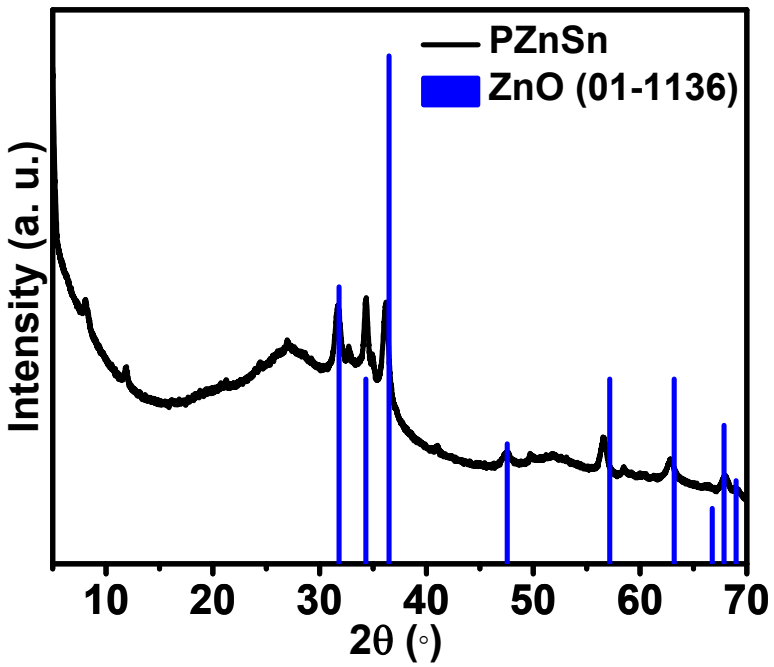

Fig. S1 XRD pattern of PZnSn with the reference peaks of ZnO

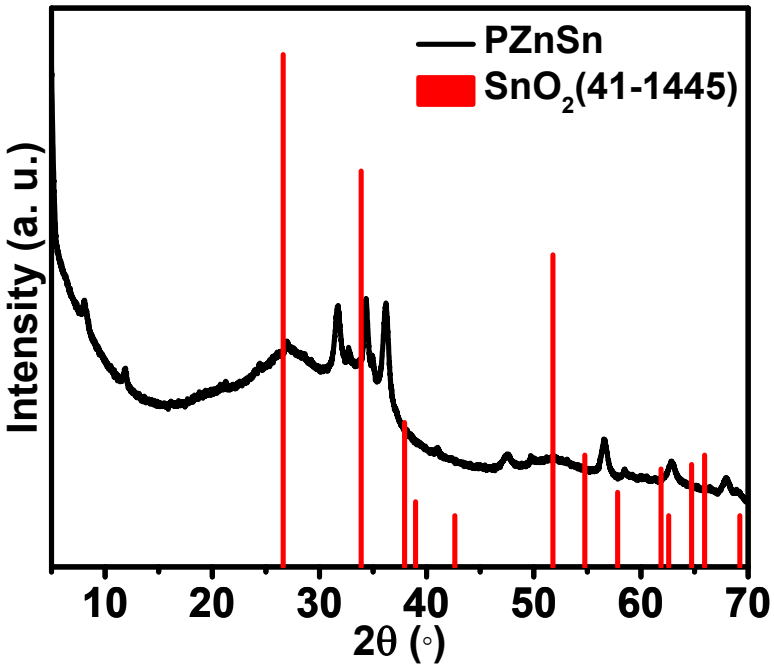

Fig. S2 XRD pattern of PZnSn with the reference peaks of SnO_2

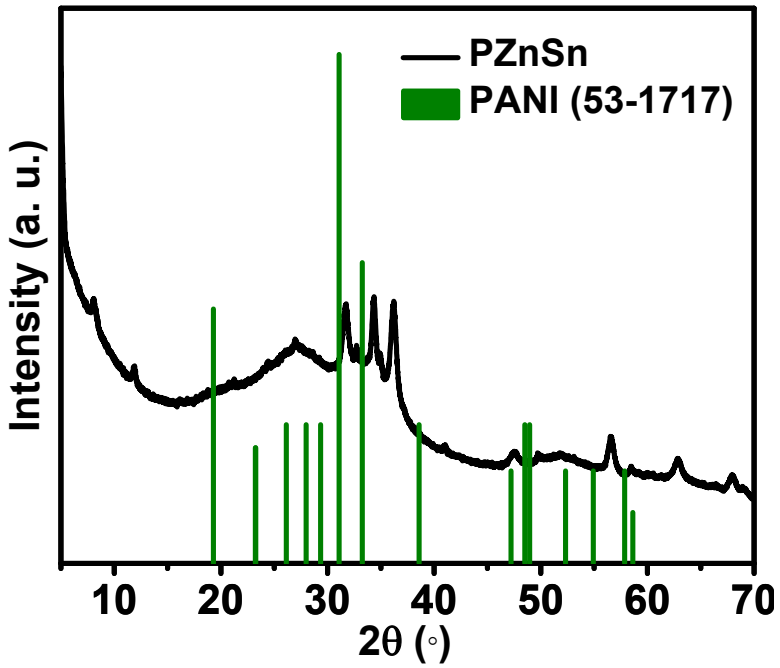

Fig. S3 XRD pattern of PZnSn with the reference peaks of PANI

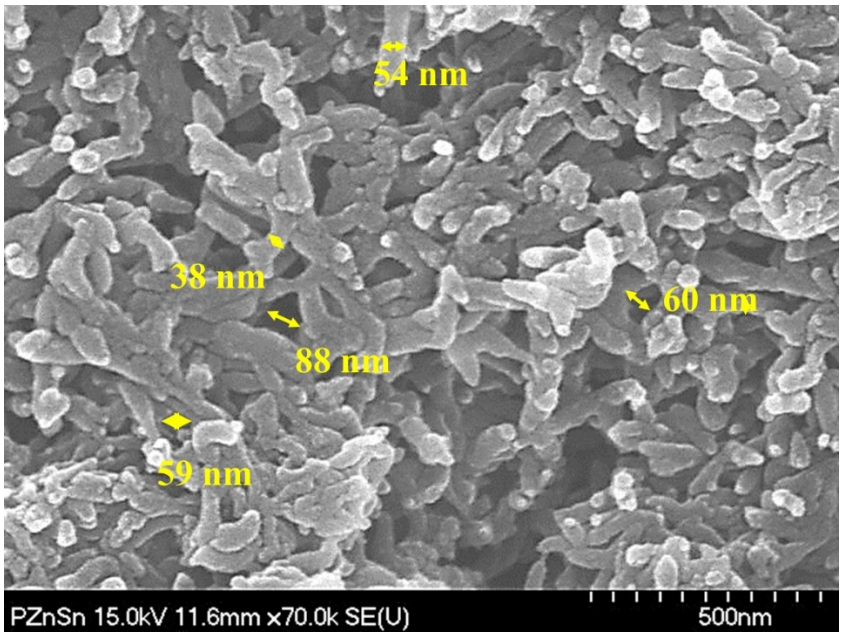

Fig. S4 The FE-SEM image of PZnSn depicting its fibre and pore diameters.

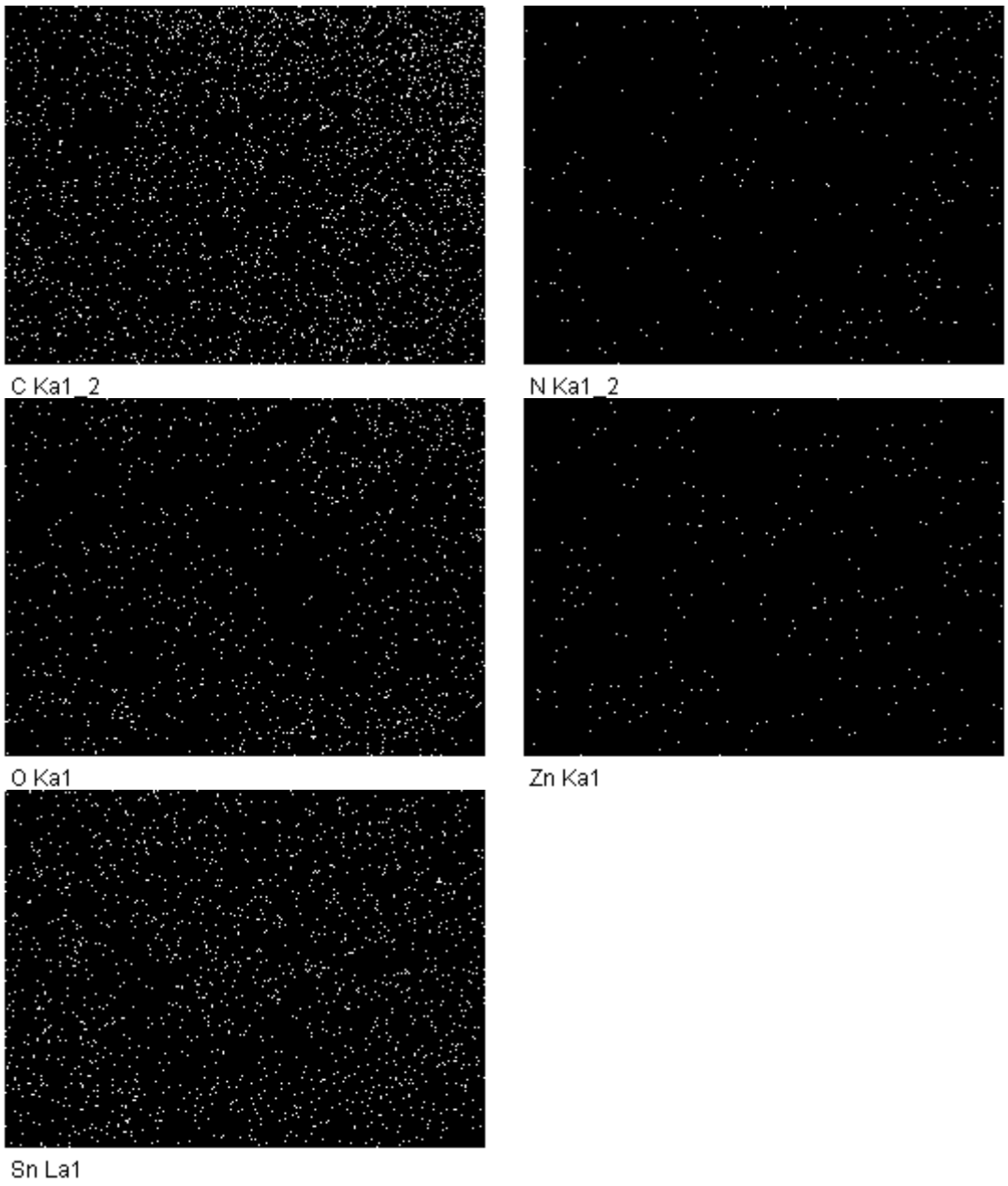

Fig. S5 The maps of different elements present in PZnSN

S4. FT-IR Spectrum of PZnSn

The transmittances at 1587, 1499, 1301, 1167, and 822 cm^{-1} (Fig. 1b) have raised due to C=C quinoid ring stretching, C=C benzenoid ring stretching, C–N stretching, C–H in-plane bending and C–H out of plane bending of PANI, respectively[1]. The transmittances at 477 [2], 523[3], and

541 cm^{-1} [3] are ascribed to the different stretching vibrations of the Sn–O bond of SnO_2. The peaks at 603 and 631 cm^{-1} are ascribed to the stretching modes of O–Sn–O [4]. The transmittances at 420[5,6], 428[7] and 452 cm^{-1} [8] are attributed to the different stretching vibrations of the Zn–O bond of ZnO.

S5. Formulae used

Specific capacity from CV curve [9,10]

$$Q = \frac{1}{2mv}\int_{vi}^{Vf} I \times V dV \qquad \text{(S1)}$$

Where, Q is the specific capacity in C g^{-1}, m is the mass of both the electrodes, v is the scan rate used and $\int_{vi}^{Vf} I \times V dV$ is the area inside the CV plot.

Specific capacity (Q in C g^{-1}) of a supercapacitor device from CD curves[9,10]

$$Q = \frac{2 \times I \times \Delta t}{m} \qquad \text{(S2)}$$

where, Q is the specific capacity (C g^{-1}), I is the constant current used for charging and discharging, Δt is the discharge time (in seconds), and m is the total mass of both electrods used.

Energy density (E in W h kg^{-1}) [9,10]

$$E = \frac{Q \times \Delta V}{2 \times 3.6} \qquad \text{(S3)}$$

Where, ΔV potential is used for charge and discharge.

Power density (P in W kg^{-1}) [9,10]

$$P = \frac{E}{t_d} \times 3600 \qquad \text{(S4)}$$

where, t_d is the discharge time at constant current.

Coulombic effecieny (η in %)[9,10]

$$\eta(\%) = \frac{t_d}{t_c} \times 100 \qquad \text{(S5)}$$

Determination of k_1 and k_2 and *deconvolution of CV curves*[20].

The energy storage processes operating in PZnSn are a combination of EDLC, redox and intercalation processes. This different charge-storing mechanism can be quantitatively differentiated by using the following concept as reported in [20].

At a given potential, the total current produced by the materials is the combination of surface capacitive current (both redox and electrical double layer processes) and diffusion-controlled ion intercalation processes,

$$i(V) = k_1 v + k_2 v^{1/2} \qquad \text{(S6)}$$

On rearranging,

$$i(V)/v^{1/2} = k_1 v^{1/2} + k_2 \qquad \text{(S7)}$$

Where, $i(V)$ is the current produced at a potential V, v is the scan rate, k_1 is the quantity of surface capacitive contribution, and k_2 is the quantity of diffusion-controlled intercalation process. The k_1 and k_2 are obtained by plotting the graph between the $i(V)/v^{1/2}$ (y-axis) and $v^{1/2}$ (x-axis), and the linear fitment of the graph provides the k_1 and k_2 in the form of slope and y-intercept as the Equation (S7) is obeying the equation of $y = mx + c$.

b-value and its significance

$$i_p = a\upsilon^b \qquad \text{(S8)}$$

i_p is peak current (A), v is the scan rate mV $s^{-1,}$ and a & b are fitting parameters. The b value is determined from the slope of the plot of log i_p vs log scan rate. The b ~0.5, indicates the faradaic intercalation process and the b=,1 indicates the capacitive process [11].

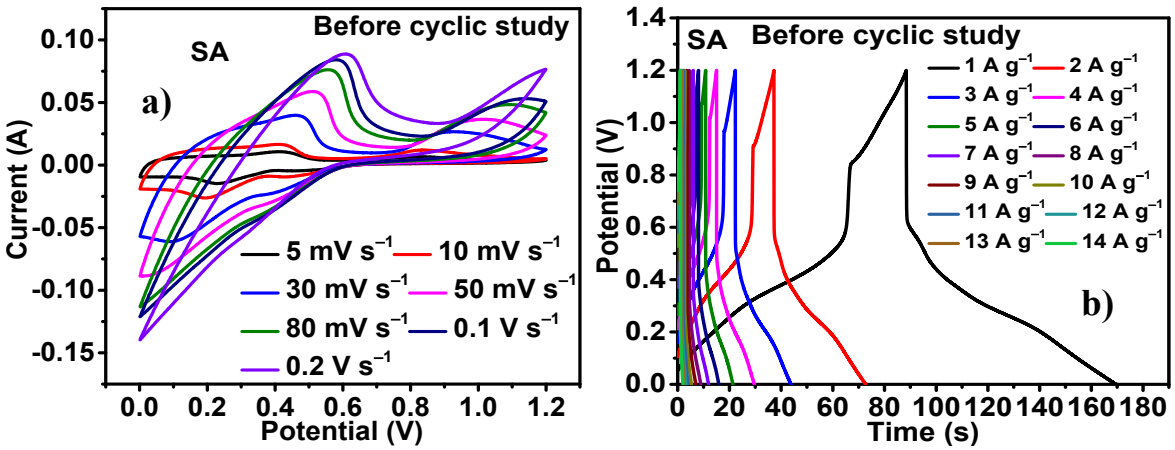

Fig.S6 a) CV curves at different scan rates and b) CD curves at different current densities of PZnSn in the presence of SA.

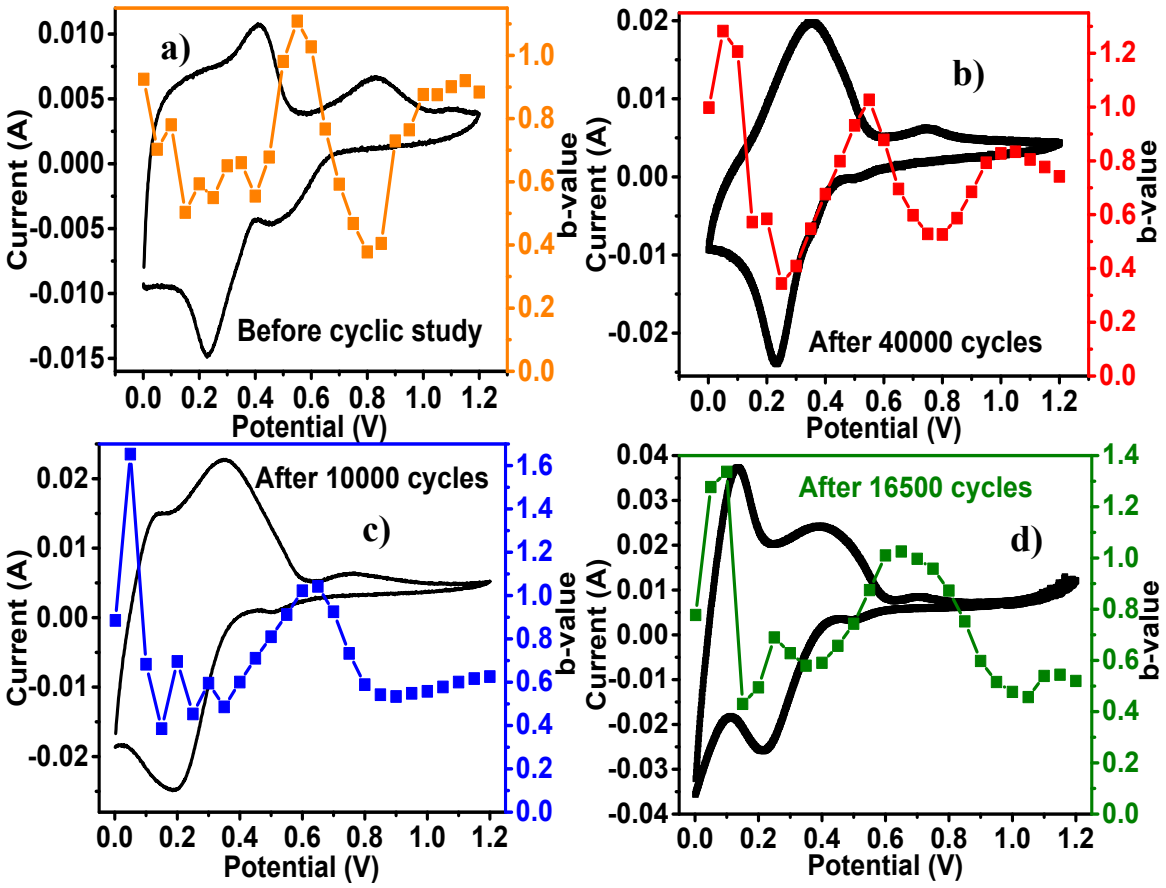

Fig. S7 Comparison of the CV curves (5 mV s^{-1}) of PZnSn obtained ITP of SA a) before the cyclic study, after b) 4000, c) 10,000 and d) 16,500 cycles with the respective *b*-value *vs*. potential plots.

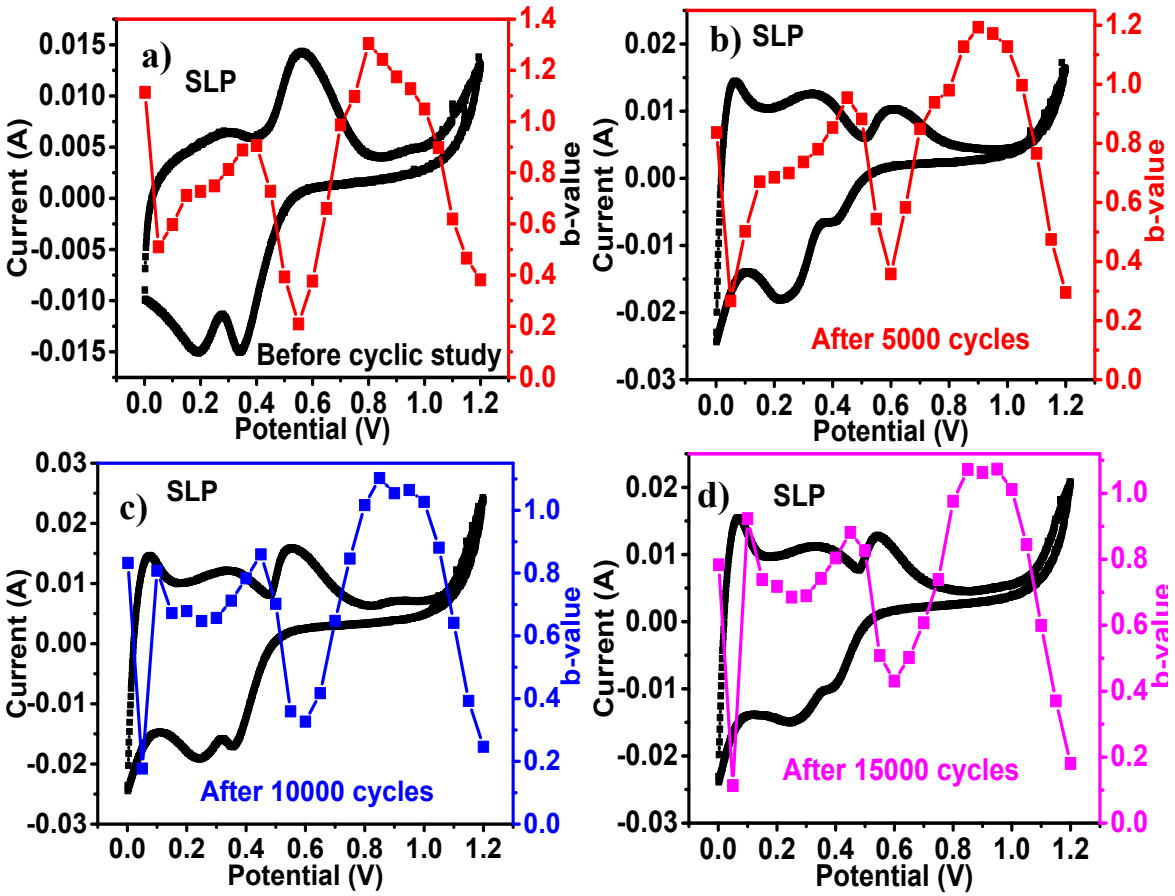

Fig. S8 Comparison of the CV curves (5 mV s^{-1}) of PZnSn obtained ITP of SLP a) before the cyclic study, after b) 4000, c) 10,000 and d) 16,500 cycles with the respective *b*-value *vs*. potential plots.

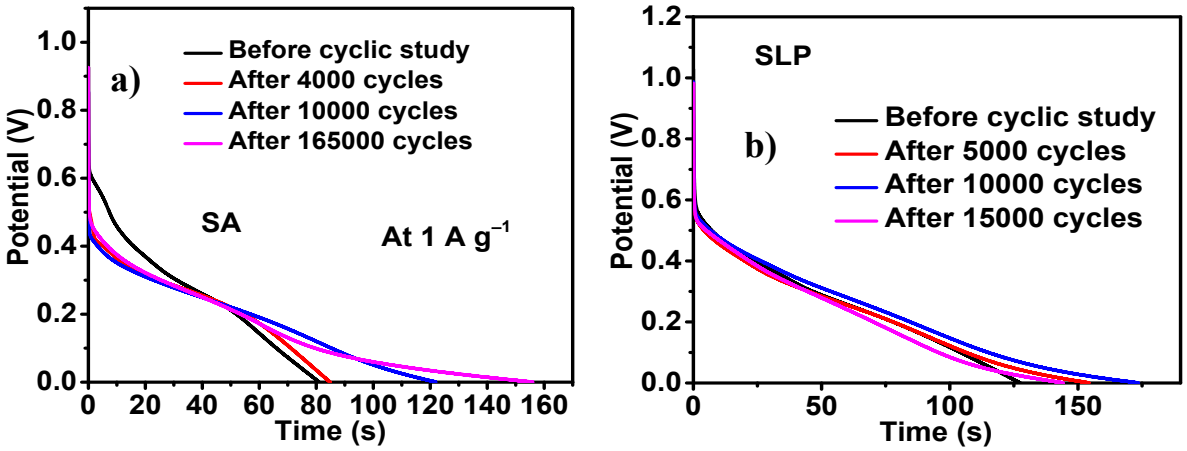

Fig. S9 The discharge curves of PZnSn show the increase of discharge time with an increase in number of cycles ITP a) SA and b) SLP.

S6. ***Descriptions of electrical elements involved in equivalent circuit***

$R_s(R_{ct}Q_1)((R_{leak}C_{dl})(Q_2))W$

The electrical elements involved are solution resistance (R_s) - a resistance that emerges from the electrolyte used; charge transfer resistance (R_{ct}) - the resistance against the transport of charges across electrolyte and electrode material, and across electrode materials and current collector, leakage resistance (R_{leak}) - the resistance due to loss of potential from the system when not connected with an external circuit or a load, Warburg diffusion resistance (W) - the resistance against the diffusion of electrolyte ions into the electrode material, the electrical double layer capacitance (C_{dl}) at the interface between the electrode material and electrolyte, constant phase elements (Q_1 and Q_2). Q_1 and Q_2 are used in place of the ideal capacitors C_1 and C_2 because the rough surface of the electrode material causes frequency dispersion during the measurement, causing the depressed semicircle at high-frequency region instead of a perfect semicircle, thereby making the capacitor to deviate from its ideality. The following Eqn relates the ideal capacitor to the constant phase element. S9.

$$C = Q(\omega_{\max})^{n-1} \quad \text{(S9)}$$

where ω_{max}, is the frequency corresponding to the maximum of the imaginary part (Z'') and n is the roughness factor (n = 0, ideal resistor, n = +1, ideal capacitor), which is a measure of the surface inhomogeneity of the electrode material [12] ($n_1 = 0.99$ and $n_2 = 0.52$).

Relaxation time (τ_0) from Bode phase angle plot

where, t_c and t_d are the charging and discharge times (in s).

$$\tau_0 = \frac{1}{f_0} \quad \text{(S10)}$$

where, f_0 is the critical frequency, corresponding to phase angle of –45°.

Capacitance (C in F) from electrochemical impedance spectroscopy

$$C = \frac{-1}{2\pi f Z''} \quad \text{(S11)}$$

where, f is the frequency (Hz) and Z'' is the imaginary part of the impedance (Ω).

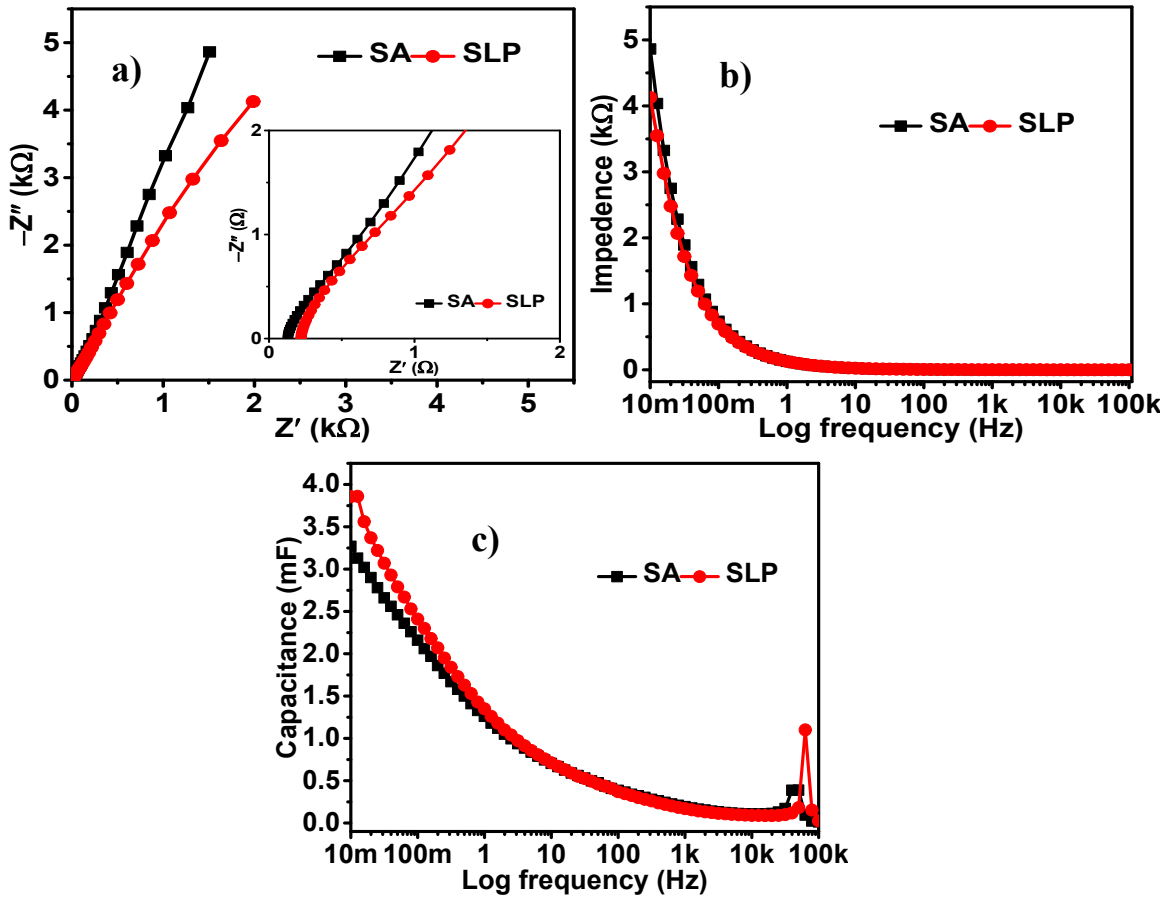

Fig. S10 a) Nyquist plots, b) Bode impedance plot and c) capacitance *vs*. log frequency plots of devices that contain electrolytes (SA and SLP), separator and current collector.

References

[1] A. Viswanathan, A.N. Shetty, Influence of different dopants and redox forms of PANI in its crystal structure, morphology, electrochemical energy storage to variable extent, unique properties and kinetics, Bull. Mater. Sci. 45 (2022) 60. https://doi.org/10.1007/s12034-021-02626-9.

[2] T. Krishnakumar, N. Pinna, K.P. Kumari, K. Perumal, R. Jayaprakash, Microwave-assisted synthesis and characterization of tin oxide nanoparticles, Mater. Lett. 62 (2008) 3437–3440. https://doi.org/10.1016/j.matlet.2008.02.062.

[3] D. Amalric-Popescu, F. Bozon-Verduraz, Infrared studies on SnO2 and Pd/SnO2, Catal. Today 70 (2001) 139–154. https://doi.org/10.1016/S0920-5861(01)00414-X.

[4] J. Zhang, L. Gao, Synthesis and characterization of nanocrystalline tin oxide by sol–gel method, J. Solid State Chem. 177 (2004) 1425–1430. https://doi.org/10.1016/j.jssc.2003.11.024.

[5] R.M. Alwan, Q.A. Kadhim, K.M. Sahan, R.A. Ali, R.J. Mahdi, N.A. Kassim, A.N. Jassim, Synthesis of zinc oxide nanoparticles via sol–gel route and their characterization, Nanosci. Nanotechnol. 5 (2015) 1–6.

[6] V. Prasad, C. D'Souza, D. Yadav, A.J. Shaikh, N. Vigneshwaran, Spectroscopic characterization of zinc oxide nanorods synthesized by solid-state reaction, Spectrochim. Acta. A. Mol. Biomol. Spectrosc. 65 (2006) 173–178. https://doi.org/10.1016/j.saa.2005.10.001.

[7] Z. Yang, Z. Ye, Z. Xu, B. Zhao, Effect of the morphology on the optical properties of ZnO nanostructures, Phys. E Low-Dimens. Syst. Nanostructures 42 (2009) 116–119. https://doi.org/10.1016/j.physe.2009.09.010.

[8] S. Fakhari, M. Jamzad, H. Kabiri Fard, Green synthesis of zinc oxide nanoparticles: a comparison, Green Chem. Lett. Rev. 12 (2019) 19–24. https://doi.org/10.1080/17518253.2018.1547925.

[9] M.Z. Iqbal, M.M. Faisal, S.R. Ali, M. Alzaid, A facile approach to investigate the charge storage mechanism of MOF/PANI based supercapattery devices, Solid State Ion. 354 (2020) 115411. https://doi.org/10.1016/j.ssi.2020.115411.

[10] M.Z. Iqbal, M.M. Faisal, M. Sulman, S.R. Ali, A.M. Afzal, M.A. Kamran, T. Alharbi, Capacitive and diffusive contribution in strontium phosphide-polyaniline based supercapattery, J. Energy Storage 29 (2020) 101324. https://doi.org/10.1016/j.est.2020.101324.

[11] J. Wang, J. Polleux, J. Lim, B. Dunn, Pseudocapacitive Contributions to Electrochemical Energy Storage in TiO2 (Anatase) Nanoparticles, J. Phys. Chem. C 111 (2007) 14925–14931. https://doi.org/10.1021/jp074464w.

[12] N. Dinodi, A.N. Shetty, Alkyl carboxylates as efficient and green inhibitors of magnesium alloy ze41 corrosion in aqueous salt solution, Corros. Sci. 85 (2014) 411–427. https://doi.org/10.1016/j.corsci.2014.04.052.